HIGH TEMPERATURE BEHAVIOUR OF LOW ENERGY HIGH FLUX NITRIDED Ni AND Ni20Cr SUBSTRATES

Fernando Pedraza, M. Reffass, J. Balmain, G. Bonnet, J.F Dinhut

HIGH TEMPERATURE BEHAVIOUR OF LOW ENERGY HIGH FLUX NITRIDED Ni AND Ni20Cr SUBSTRATES

*F. Pedraza, M. Reffass, J. Balmain, G. Bonnet and J.F. Dinhut**

LEMMA, Université de La Rochelle. 25, rue Enrico Fermi. 17042 La Rochelle cedex 1. France.

** corresponding author : Phone: +33 (0)546458219, Fax: +33 (0)546457272, e-mail: jfdinhut@univ-lr.fr*

Abstract

Nitridation at low energy- high flux implantation-diffusion has been performed on pure Ni and Ni20Cr substrates in order to study their high temperature oxidation behaviour at 700 and 800° C in synthetic air. The nitridation treatment has led to significant sputtering on pure Ni, but no implanted nitrogen has been detected. On the contrary, the Ni20Cr substrates are able to incorporate nitrogen, with less sputtered surfaces. Porosity is anyhow found on both substrates after the nitridation treatment. No particular difference is found to occur on the oxidation kinetics of Ni specimens but on their scales morphology. On the contrary, in Ni20Cr specimens, oxidation is enhanced mainly upon the first exposure times owing to trapping of chromium by the implanted nitrogen. Furthermore, the expanded austenite γ_N layer formed on the nitrided Ni20Cr samples is stable up to 700°C for 24 h, after which evolution towards the nitride precipitation occurs.

Keywords : nitridation, implantation, high temperature oxidation, nickel, Ni20Cr.

1.- Introduction

A great variety of nitridation treatments mainly on tool and stainless steels [1-7] are well known aiming to improve their surface hardness and wear resistance. Improvements in aqueous corrosion resistance have also been reported for the AISI 304 stainless steel nitrided by low energy – high flux implantation at 400° C [8]. As a result of the nitriding treatment, an "expanded austenite" γ_N layer is formed in materials with a face centred cubic structure (fcc) or M_xN_y phases appear in tool steels (M = metal with strong affinity for nitrogen).

Nitridation studies on Ni base alloys mainly concern the internal degradation after failure of the outer protective oxide scale under high temperature environments [9]. After ingress of nitrogen in the metal from a gaseous atmosphere, net volume increase attending precipitation occurs, generating stresses [10], which even lead to deformation processes such as creep [11]. Controlled internal nitridation in oxygen-free atmospheres has also been studied [12-15], the major findings indicate that the highest chromium concentrations seem to increase the solubility and diffusion of nitrogen in the Ni-base alloys. After nitridation, nickel protrusions are typically found at the outer surface.

On the other hand, nitridation treatments to enhance the wear resistance of Ni base alloys have also been documented. For instance, plasma nitriding studies have been carried out on Inconel 718 (Ni-20 wt% Cr base alloy) resulting in an increase of Knoop hardness [16] and in wear resistance [17] although this is a matter of controversy, i.e. the absence of the CrN phase in the same alloy has been claimed not to improve erosive wear [18]. More detailed studies on the plasma nitrogen diffusion have been conducted on Inconel 690 (Ni-30wt% Cr base alloy) [19,20]. In the current literature, only two works on the nitridation of Ni-base alloys by low energy-high flux nitrogen implantation have been reported using different experimental

conditions [21,22]. Regardless of this fact, both studies agree in the formation of a thinner and less nitrogen-rich layer compared to that typically formed in steels.

However, to the best of our knowledge, no study has been presented concerning the effects of the nitridation treatment on the high temperature behaviour of Ni and Ni20Cr substrates. These represent the metal matrix and model alloy (in terms of chromium content), respectively, of many Ni-base superalloys. Besides, the only study reported on the high temperature stability of the nitrided layer was conducted in argon at 450° C up to 50 h to retransform the stress-induced martensite formed upon plasma nitriding of AISI 304L stainless steel [23]. Therefore, in the present work we intend to report on the derived consequences of a low energy high flux nitridation treatment on the high temperature response of the above-mentioned substrates.

2.- Experimental Procedure

Pure Ni (99.95 % purity) and Ni20Cr (Ni-20Cr-1.5Si, wt%) (Goodfellow) polished down to 1 μm diamond paste were implanted at low energy–high flux under 1.2 keV and 1 $mA.cm^{-2}$ for 1 h conditions, delivering an estimated dose of 3.5 x 10^{19} $ions.cm^{-2}$. The temperature of the samples achieved 450 and 475 °C for Ni20Cr and Ni, respectively.

Isothermal oxidation runs were carried out in a Setaram TGA92 thermobalance (accuracy of ± 1 μg) at 700 and 800°C. A constant heating rate of 10°$C.min^{-1}$ was set under pure Ar (g) before achieving the test temperatures. After 24 h of exposure, the samples were cooled at the rate of 10°$C.min^{-1}$ under the same flow of synthetic air (0.6 $l.min^{-1}$).

Characterisation of the implanted specimens was undertaken in a Bruker AXS D-5005 diffractometer in the θ-2θ configuration, using the Cu $K_{\alpha 1}$ (λ = 0.15106 nm) and scanning electron microscopy (SEM) coupled to energy-dispersive spectrometry (EDS) in a JEOL JSM-4510 LV.

3.- Results

3.1.- Nitrogen implantation

The surface morphology of Ni and Ni20Cr after nitridation is shown in Figure 1 (a) and (b), respectively. It can be readily observed that the nitridation treatment has led to more sputtering in pure Ni than in Ni20Cr. Furthermore, the distribution of such sputtering is unequal throughout the surface and twinning occurs within some of the grains. Porosity is also a common feature for both materials after nitridation. Measurements of the mean roughness by atomic force microscopy (AFM) actually revealed values ranging from 175 and 275 Å in Ni depending on the grains, whereas on Ni20Cr specimens, the Ra values only attained about 80 Å [24]. Differences between both specimens also refer to their chemical composition since a nil nitrogen amount is obtained by EDS microanalyses on the Ni samples compared to a maximum amount of nitrogen (with Cr/N ratios of about 1) at the external nitrided layer of the Ni20Cr samples [24].

According to the XRD scans, the formation of a γ_N solid solution is absent on the Ni substrates. All these facts may imply that no nitrogen is actually incorporated to the metal matrix or if it is, its amount is under the detection limit of the techniques employed. On the contrary, the Ni20Cr is able to incorporate nitrogen into its matrix as shown by the appearance of the γ_N expanded austenite on the left of the austenite peaks of the matrix (Figure 2). A shift of the latter peaks towards higher diffraction angles is also observed. The

calculations of the lattice constants for each plane indicate that preferential solid solution of nitrogen occurs at the (200) planes. The SEM cross sections had shown that a progressive decrease of the nitrogen concentration providing an overall nitrided layer of about 3.5 μm [24].

3.2.- High temperature oxidation behaviour

Even though no nitrogen seems to have been retained in the Ni substrates, the implantation treatment may alter its high temperature behaviour. Figure 3 (a) shows the mass gain curves as a function of time for both untreated and nitrided Ni specimens. No significant difference is observed at both temperatures, especially at 800° C, where a perfect match of both curves is readily seen. Assuming parabolic behaviour, the oxidation constants have been calculated by the $(\Delta M/S)^2$ vs. time method [Figure 3 (b)], giving rise to values of $4x10^{-12}$ and $2.5x10^{-11}$ $g^2.cm^{-4}.s^{-1}$ for 700 and 800° C, respectively.

As expected after oxidation, the θ-2θ XRD patterns have revealed the formation of NiO oxides in both untreated and nitrided, together with some weak peaks of the substrate, indicating a relatively thick oxide layer at both temperatures (Figure 4). Besides, the texture of the as-received material, i.e. the {111} planes preferentially parallel to the surface, disappears after the nitridation treatment. Thus, after oxidation, no apparent preferential growth of the oxides should be expected.

Figure 5 (a) shows the development of a porous net of NiO oxides developed on the untreated Ni at 700° C (similar behaviour for the 800°C samples, not shown). However, after implantation, the surfaces show extensive spallation that might have occurred upon the oxidation treatment since a relatively dense oxide sub-layer lies beneath the porous one

[Figure 5(b)]. Besides, the appearance of a platelet-like morphology was revealed in certain areas [Figure 5(c)]. The cross sections confirm the presence of the porous nature of the layers formed on untreated Ni at both 700 and 800°C, as shown in Figures 6 (a) and (b), respectively. After implantation, layers of similar thickness are observed on untreated and nitrided specimens at each oxidising temperature, with irregular scale/substrate interfaces mainly observed at 700° C [Figures 6 (c) and (d)].

Figure 7 shows the mass gain as a function of time for the Ni20Cr substrates oxidised at 700° and 800°C for 24 h. It can be observed that nitridation involves an increase in oxidation kinetics at both studied temperatures. Assuming parabolic behaviour, the parabolic constants have been calculated and they are presented in Table 1.

The parabolic rate constants of the untreated material reflect the effects of increasing temperature. Indeed, the k_p values are one order of magnitude higher at 800°C than at 700°C at the end of the experiments. The most significant distinction corresponds to the appearance of a transition stage at 700° C in which oxide development may be governed by the development of more than one oxide phase.

In the nitrided specimens, the complexity of oxide growth processes hinders any accurate linear fit from 0 to 10 h of exposure in the $(\Delta M/S)^2$ vs. time plots. However, for the longest exposures, a difference of more than one order of magnitude of the k_p values is obtained between the untreated and the nitrided specimens. Overall, direct comparison between the untreated and nitrided samples at the different temperatures and for the final times clearly indicates that oxidation is somewhat enhanced after implantation.

The oxide species developed on Ni20Cr are the same for both the untreated and nitrided specimens at either temperature and these include NiO, $NiCr_2O_4$ and Cr_2O_3, as assessed by XRD. The differences on intensity of these oxide species are in agreement with the temperatures employed, i.e. at the highest temperatures, more contribution of Cr_2O_3 oxide is found to occur. However, the substrate/oxide intensity ratios are always higher at any temperature than in the nickel substrates, which is in agreement with the TGA experiments [compare Figures 3 and 7]. This means that a thinner oxide layer is obtained in the Ni20Cr samples after 24 h of isothermal oxidation.

The most interesting feature highlighted by XRD is the presence of the expanded austenite phase (γ_N) after oxidation at 700°C, which had been formed after nitridation (see Figure 2). Typically, the insertion of nitrogen in a face centred cubic structure (fcc) leads to a doublet of the original γ peak [e.g. 21]. A shift to lower angles corresponds to the lattice expanded by the interstitial nitrogen, whereas a shift to higher angles indicates the "contracted" remaining austenitic lattice. The higher the nitrogen content, the higher the shift to lower angles of the γ_N phase and vice-versa. After implantation, nitrogen preferentially concentrates at the (200) planes (bigger $2\theta\gamma$-2θ γ_N difference). After oxidation at 700°C for 24 h, the γ_N and γ peaks shift towards the original γ phase ($2\theta = 44.28°$) giving rise to the observed doublet. This clearly imply redistribution of nitrogen in the matrix but no nitride phase can be derived from the XRD results.

However, according to the surface compositions obtained by EDS, diffusion of the main species composing the oxide layer remains unchanged (see Figure 8) at 700°C. Only outward Ni diffusion seems to be promoted at 800°C on the nitrided samples.

The surface sputtering created on the surfaces upon the implantation process changes nevertheless the oxide morphologies, as assessed by SEM. The untreated Ni20Cr specimens develop a homogeneous and relatively dense oxide layer composed of tiny crystals at both oxidising temperatures after 24 h, as those shown in Figure 9 (a). On the contrary, the nitrided samples show preferential oxidation depending on the grain orientation and grain and/or twin boundary induced upon implantation. The evolution of such oxide films grown on nitrided specimens at 700 and 800°C is shown in Figures 9 (b) to (e). At the lowest temperatures, the samples are distinctively covered of oxides, which are more developed at 800°C. At this temperature, the appearance of platelet oxides is clearly observed which seem to follow different crystallographic orientations within the grains [Figure 9 (e)].

The cross sections of the untreated samples do not reveal any special feature after oxidation, with scales growing continuously from the substrate surface and a certain internal growth. This is a common feature with the nitrided materials but in the latter, a more wavy scale/substrate interface has developed owing to the surface roughness after implantation. Generally, the scale thicknesses are larger in the nitrided materials. No particular morphology is observed after 700°C (which contains some nitrogen beneath the oxide scale/matrix interface) in contrast to the 800°C samples, in which a band of precipitates of about 8 μm extends inwardly from the scale/substrate interface [see Figure 10 (a)]. The EDS microanalyses of these precipitates zone reveal decreasing nitrogen contents towards the substrate matrix [Figure 10 (b)].

4.- Discussion

4.1.- Nitrogen implantation

The XRD patterns and the EDS microanalyses have shown the absence of implanted nitrogen using the present experimental conditions in nickel substrates. Indeed, it is well known that nitrogen solubility in nickel is extremely low [25]. Further, saturation of nitrogen concentration in nickel has been recently shown by Auger electron spectroscopy (AES) to occur using either hydrazoic acid or ion implantation. A decrease in nitrogen is, in any case, obtained at temperatures above 375° C owing to the loss of this element from the transition metal nitrides [26]. Besides, the implanted dose ($3.5x10^{19}$ at.cm^{-2}) of the present study exceeds the atomic concentration Ni may incorporate in solid solution ($2.5x10^{19}$ at.cm^{-2}, as calculated from its lattice parameter). According to these arguments, some porosity occurs, as revealed in Figure 1, which thus results from a combination of two main parameters: (a) nickel does not dissolve important amounts of nitrogen, which then recombines inside the substrate in the form of bubbles so as to minimise the nitrogen/nickel interfacial energy, and (b) upon implantation, surface sputtering occurs, thus the real surface retracts. Owing to the initially textured nickel, sputtering occurs preferentially in some of the grains, peeling off both the substrate and the occluded porosity.

On the contrary, nitrogen has been observed to remain in the Ni20Cr substrates, which leads to the appearance of a γ_N phase on the XRD patterns. This peak is more shifted to lower angles in the case of the (200) reflections compared to the (111), which is in agreement with most of the investigations undertaken on homologous ~ 20 wt% Cr-containing stainless steels, as the AISI 304 family [4,7,21,23] or the AISI 316 [27].

According to the mechanism suggested by Möller et al. [28], in which chromium atoms trap and de-trap the implanted nitrogen, more nitrogen should have been found in this case, i.e. similar amounts of chromium and nitrogen at any location. However, the effect of radiation also has to be considered at temperatures above 350° C at which vacancies are mobile [29] and thus both nickel and chromium are transported outward. A counter-current effect is thus played by nickel rejecting nitrogen and chromium trapping it. In any likely mechanism, porosity is also found on the surface of the Ni20Cr substrates, as explained above for the nickel specimens.

4.2.- High temperature oxidation behaviour

a) Ni samples

Owing to the likely absence of implanted nitrogen in the nickel specimens, no chemical contribution has been expected to occur but a mechanical one. It has been shown however, that oxidation takes place in a similar manner on both untreated and treated samples in what oxidation kinetics are concerned. The calculated parabolic rate constants are $5x10^{-12}$ and $2.5x10^{-11}$ $g^2.cm^{-4}.s^{-1}$ with final oxide thickness of about 5 and 10 μm at 700 and 800° C, respectively. This implies that at 700° C, the oxide layers grown on 1 μm polished nickel have double values than those assessed by impedance spectroscopy on 1200 ground specimens after 20 h of oxidation at 700° C [30,31]. However, this is in contradiction with the findings of Huntz et al. [32] on the oxidation of pure nickel at 800° C, in which the greater the substrate surface roughness, the greater the oxidation rate owing to the enhancement of nickel injection in the oxide films.

The parabolic constant values agree well to those recently published by Peraldi et al. [33] for the same fixed oxide layer thickness. The slight differences can be explained in terms of the

different oxidising atmospheres (synthetic air in our study vs. pure oxygen in their study) and also the method of k_p evaluation since they employed a more precise and complete expression. In any case, deviations from linearity of the ΔM vs. $t^{1/2}$ plots have been observed to occur for the first oxidation times. On the other hand, our experimental k_p value at 700° C is one order of magnitude lower than the one reported by R. Haugsrud [34] which was found to be independent of the oxygen partial pressure but is similar for the 800° C temperature. However, this author claimed that the rate constants at 700° C were more of a qualitative matter owing to the different behaviour actually encountered between the first and the latter oxidation times.

The microstructure of the NiO scales developed on untreated nickel samples have shown the formation of cellular oxides at either 700 and 800° C. Nonetheless, more apparent coverage on certain grains of this untreated substrate is observed especially at 700° C as a direct result of the relatively textured initial structure of the as-received nickel, but oxide growth anisotropy is anyhow a well known feature of NiO oxides [35-38]. However, at 800° C some isolated areas contained platelets growing outwardly from the cellular oxide scale. The development of such platelets is clearly enhanced after oxidation of the implanted specimens. In fact some of the grains are fully covered of these oxides [cf. Figure 5(c)] even at 700°C. The extent of the platelets is afterwards increased at 800° C (not shown). According to the microstructure maps established for nickel oxidised at different temperatures and times [39], at 700° and 800°C and 24 h of oxidation, intersection between the cellular and platelet morphologies fields should occur, which agrees to a certain extent with our observations. Peraldi et al. [39] consider that the origin and growth of the platelets seem to be inherent to the scale growth process with no dependence on specific defects in the substrate or the scale/metal interface. However, in our experimental work, no nitrogen has been found on the

surfaces of nickel but strong sputtering has preferentially occurred in certain grains which have led to the development of the platelet-like oxides. These may grow by preferential outward cation diffusion owing to their location at the outermost cellular scale surface.

The double configuration typically reported on NiO scales with an outer columnar structure above a fine equiaxed layer [e.g. 34,40] is quite difficult to appreciate in the SEM polished cross sections but it seems to be better developed on the treated samples after oxidation at 800° C indicating a predominant cation flux at the first oxidation times.

b) Ni20Cr samples

Two distinct oxidation behaviours have been observed at 700 and 800° C on the untreated materials. For the shortest times, oxidation proceeds faster than for the latter. Although parabolic behaviour has been assumed, it is known that this is only encountered at the very early stages. From then on, a complete law should be considered [33]. Our experimental values of $1x10^{-15}$ and $2.3x10^{-14}$ $g^2.cm^{-4}.s^{-1}$ at 700 and 800°C, respectively, agree well with those obtained by Calvarin and co-workers [41,42] on 200 μm thick Ni20Cr thin strips. The slight differences can be mainly explained in terms of the presence of 1.5 wt% Si compared to 0.085 wt% Si of their studies. Even if, overall, Si has been reported to promote scale adherence and decrease of oxide kinetics, the presence of this element enhances heterogeneous nucleation of the subsequently growing oxide layers at short oxidation times [43].

On nitrided samples, no accurate linear fit could be performed on the $(\Delta M/S)^2$ plots indicating the complexity of the oxidation mechanisms owing to the implantation treatment. For instance, Giggings and Pettit [44] already studied the effect of alloy grain size and surface

deformation on Ni-Cr alloys at higher temperatures than ours and concluded that deformation produced more grain boundaries along which chromium could be selectively oxidised. After the non parabolic behaviour of the first stages, the k_p values have been calculated for the final oxidation times (10-24 h) giving values about one order of magnitude higher both at 700 and 800° C than the corresponding untreated materials. This, in fact is related to such enhanced oxidation observed during the first times. Indeed, direct comparison of each set of ($\Delta M/S$) curves for a given temperature reveal that at the latter stages, the untreated and treated curves are parallel and so, oxidation might proceed similarly.

In any case, the oxide species developed on both untreated and nitrided substrates are the same : NiO, $NiCr_2O_4$ and Cr_2O_3, the intensity of each varying with oxidation temperature and treatment. For instance, chromia is better developed at 800 than at 700° C, in agreement with G. Calvarin [41], irrespective of the untreated or nitrided nature of the sample. However, nickel outward transport seems to be promoted at 800° C on the nitrided specimens, as it has been assessed by EDS microanalyses and the SEM observations, with platelet-like oxides growing at the outermost scale surface normal to it. Studies on internal nitridation of nickel base alloys have shown outward diffusion of nickel, which have been explained by the volume increase induced by nitride formation and subsequent internal compressive stresses [e.g. 10]. This feature is similar to the results obtained for the nitrided nickel specimens and is in common agreement with the observations of Peraldi et al. [39].

The typical sandwich structure (outer NiO/central $NiCr_2O_4$/inner Cr_2O_3) [45-48] has been difficult to assess owing to the thin nature of the layers developed but oxidation is observed to be enhanced through grain and twin boundaries (bigger density after nitridation) upon oxidation, as well as within certain grains (volume diffusion). However, the difference in

chromia contents of the untreated and nitrided scales obeys to the presence of nitrogen. Whereas at 700° C, nitrogen might have diffused inwardly thus reducing its concentration at the most external substrate layer, i.e. γ_N shift towards higher angles avoiding coarse precipitation, at 800° C such precipitates have been found to occur through a relatively thick band. Thus, even if initial deformation may enhance chromium diffusion as previously suggested [44], this element is relatively trapped probably forming nanoprecipitates already at 700°C and TEM studies should be conducted to confirm this possibility. Anyhow, since the retained amounts of nitrogen which harden the surface [24] are not of significant importance, enough flux of chromium from the matrix occur, decreasing the overall oxidation kinetics at the longest exposures.

5.- Conclusions

Implantation-diffusion of nitrogen has been shown to introduce stronger sputtering on Ni than on Ni20Cr. The remaining porosity is explained in terms of excess of dose and rejection of nitrogen from nickel at the implanting temperatures. No nitrogen is thus incorporated in the pure nickel substrates while some amounts of nitrogen remain implanted in the Ni20Cr specimens.

The high temperature behaviour of nickel does not basically change after implantation in what oxidation kinetics are concerned. However, a change of oxide scale morphology is observed with more density of NiO external platelets growing normal to the cellular morphology.

The presence of nitrogen on Ni20Cr samples does influence the kinetics by increasing one order of magnitude their oxidation. This is mainly found to be a result of chromium trapping owing to chromium nitride precipitation at 800°C. At lower temperatures, no precipitation has

been found but this possibility is not excluded. In any case, for the longest exposures enough chromium flux from the matrix seems to be ensured.

6.- Acknowledgements

Special thanks are directed to Mr. G. Abrasonis and Prof. Rivière (UMR-6630, Poitiers, France) for performing the nitridation experiments. The authors would also like to thank the Centre Commun d'Analyses of the Université de La Rochelle for their kind help. Funding of the post doctoral stay of F. Pedraza is especially acknowledged to the Region of Poitou-Charentes (France).

7.- References

1. R. Wei, Surf. Coatings Technol. 83 (1996) 218.
2. P.J. Wilbur, J.A. Davis, R. Wei, J.J. Vajo, D.L. Williamson, Surf. Coatings Technol. 83 (1996) 250.
3. S.J. Bull, A.M. Jones, A.R. McCabe, Surf. Coatings Technol. 83 (1996) 257.
4. A.M. Jones, S.J. Bull Surf. Coatings Technol. 83 (1996) 269.
5. B.S. Mann, B. Prakash, Wear 240 (2000) 223.
6. N. Renevier, P. Collignon, H. Michel, T. Czewiec, Surf. Coatings Technol. 111 (1999) 128.
7. C. Blawert, H. Kalvelage, B.L. Mordike, G.A. Collins, K.T. Short, Y. Jiraskova, O. Schneeweiss, Surf. Coatings Technol. 136 (2001) 181.
8. S. Picard, J.B. Memet, R. Sabot, J.L. Grosseau-Poussard, J.P. Rivière, R. Meilland, Mater. Sci; Eng. A 303 (2001) 163.
9. J.X. Dong, K. Sawada, K. Yokokawa, F. Abe, Scripta Mater. 44 (2001) 2641.
10. S.Y. Chang, U. Krupp, H.J. Christ, Mater. Sci. Eng. A 301 (2001) 196.

11. G.C Sava, G.C. Weatherly, J.S Kirkaldy, Scripta Mater. 34 (1996) 1087.
12. A.A. Kodentsov, J.H. Gulpen, C. Cserhati, J.K. Kivilahti, F.J.I. Van Loo, Met. Mater. Trans. 27A (1996) 59.
13. U. Krupp, H.J. Christ, Oxid. Met. 52 (1999) 277.
14. U. Krupp, H.J. Christ, Oxid. Met. 52 (1999) 299.
15. U. Krupp, H.J. Christ, Met. Mater. Trans. 31A (2000) 47.
16. P.K. Aw, A.W. Bachelor, N.L. Loh, Surf. Coatings Technol. 89 (1997) 70.
17. P.K. Aw, A.W. Bachelor, N.L. Loh, Wear 208 (1997) 226.
18. V. Shanov, W. Tabakoff, Surf; Coatings Technol. 86-87 (1996) 88.
19. C. Leroy, T. Czerwiec, C. Gabet, T. Belmonte, H. Michel, Surf. Coatings Technol. 142-144 (2001) 241.
20. H. He, T. Czerwiec, C. Dong, H. Michel, Surf. Coatings Technol. (2002), in press.
21. D.L. Williamson, J.A. Davis, P.J. Wilbur, Surf. Coatings Technol. 103-104 (1998) 178.
22. J.P. Rivière, P. Méheust, J.A. García, R. Martínez, R. Sánchez, R. Rodríguez, Surf. Coatings Technol. 158-159 (2002) 295.
23. E. Menthe, K.T. Rie, Surf. Coatings Technol. 116-119 (1999) 199.
24. F. Pedraza, M. Reffass, C. Savall, G. Abrasonis, J.P. Rivière, J.F. Dinhut, Surf. Coatings Technol. submitted for publication.
25. M.Hansen, K. Anderko, Constitution of Binary Alloys, 2nd Ed. McGraw-Hill, New York, 1958, p. 984.
26. K. Han, D.H. Fairbrother, Appl. Surf. Sci. 195 (2002) 229.
27. M.P. Fewell, D.R.G. Mitchell, J.M. Priest, K.T. Short, G.A. Collins, Surf. Coatings Technol. 131 (2000) 300.
28. W. Möller, S. Parascandola, T. Telbizova, R. Günzel, E. Richter, Surf. Coatings Technol. 136 (2001) 73.

29. L. Pranevicious, C. Templier, J.P. Rivière, Ph. Méheust, L.L. Pranevicious, G. Abrasonis, Surf. Coatings Technol. 135 (2001) 250.
30. S.H. Song, P. Xiao, Scripta Mater. 44 (2001) 601.
31. S. Song, P. Xiao, Mater. Sci. Eng. A323 (2002) 27.
32. A.M. Huntz, B. Lefevre, F. Cassino Mater. Sci. Eng. A290 (2000) 190.
33. R. Peraldi, D. Monceau, B. Pieraggi, Oxid. Met. 58 (2002) 275.
34. R. Haugsrud, Corr. Sci. 45 (2003) 211.
35. H. Li, F. Czerwinski, A. Zhilyaev, J.A Spuznar, Corr. Sci. 39 (7) (1997) 1211.
36. F. Czerwinski, J.A. Spuznar, Corr. Sci. 39 (8) (1997) 1459.
37. F. Czerwinski, J.A. Spuznar, Corr. Sci. 41 (1999) 729.
38. M.J. Graham, R.J. Hussey, Corr. Sci. 44 (2002) 319.
39. R. Peraldi, D. Monceau, B. Pieraggi, Oxid. Met. 58 (2002) 249.
40. P. Berger, L. Gaillet, R. El Tahhann, G. Moulin, M. Viennot, Nucl. Inst. Meth. Phys. Res. B 181 (2001) 382.
41. G. Calvarin-Amiri, PhD Thesis, University of Paris XI-Orsay (1998).
42. G. Calvarin, R. Molins, A.M. Huntz, Oxid. Met. 53 1 /2 (2000) 25.
43. F.J. Pérez, E.Otero, M.P. Hierro, C. Gómez, F. Pedraza, J.L. de Segovia, E. Román, Surf. Coatings Technol. 108-109 (1997) 127.
44. C.S. Giggings, F.S. Pettit, Trans. Met. Soc; AIME 245 (1969) 2509.
45. C.S. Giggings, F.S. Pettit, Trans. Metal. Soc. AIME, 245 (1969) 2495.
46. T. Amano, O. Momose in Y. Saito, B. Önay, T. Maruyama (Eds.), High Temperature Corrosion of Advanced Materials and Protective Coatings, Elsevier Science Publishers, 1992, p. 111.

47. T. Amano, O. Momose, in Y. Saito, B. Önay, T. Maruyama (Eds.), High Temperature Corrosion of Advanced Materials and Protective Coatings, Elsevier Science Publishers, 1992, p. 163.
48. G. Calvarin-Amiri, A.M. Huntz, R. Molins Mater. High Temp. 18(2) (2001) 91.

Table 1.- Parabolic rate constants (k_p) of the untreated and nitrided Ni20Cr after their oxidation at 700° and 800°C for 24 h under synthetic air.

	T, °C	time span, h	k_p, $g^2.cm^{-4}.s^{-1}$
untreated	700	0-16	5.3×10^{-14}
		16-20	transition
		16-24	1.0×10^{-15}
	800	0-13	6.2×10^{-14}
		13-24	2.3×10^{-14}
nitrided	700	0-10	no linear fit
		10-24	8.3×10^{-15}
	800	0-10	no linear fit
		10-24	2.3×10^{-13}

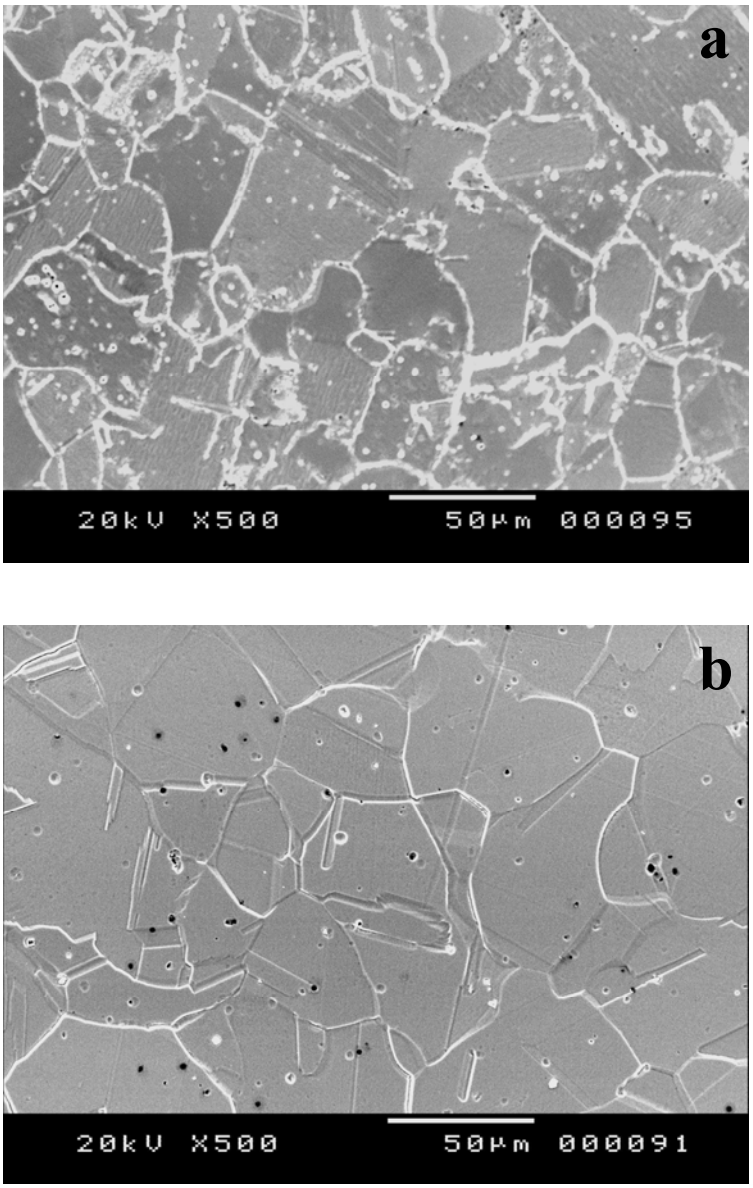

Figure 1.- SEM surface morphologies of the nitrided (a) Ni and (b) Ni20Cr substrates.

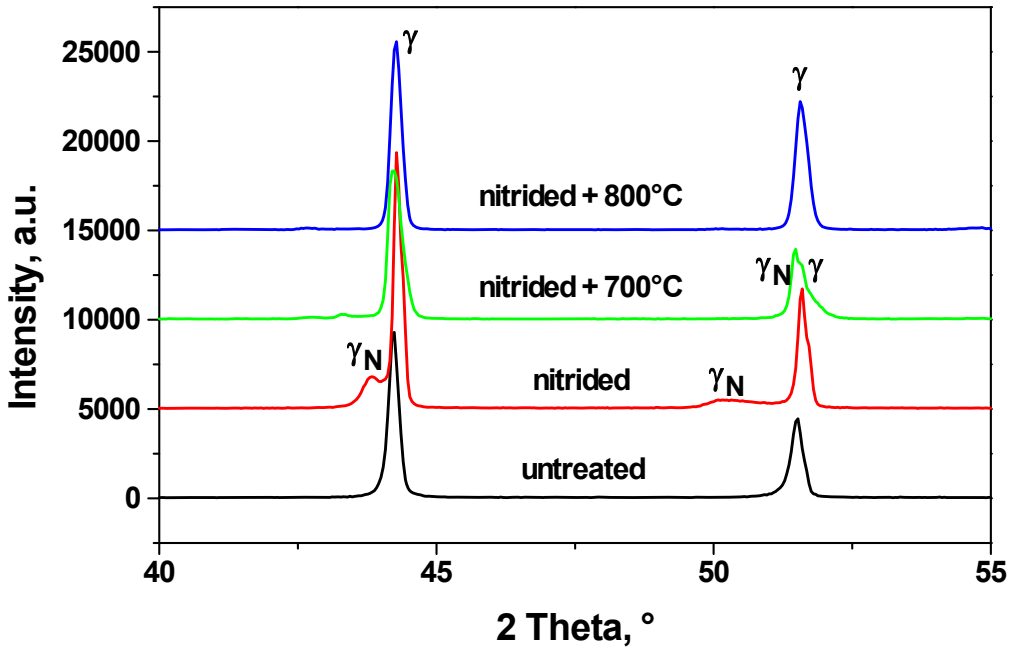

Figure 2.- Selected range of the XRD patterns obtained on the untreated, as-nitrided and nitrided and oxidised at 700° and 800°C Ni20Cr substrates. N.B: Only the matrix peaks are indicated. See text for further information concerning oxide species.

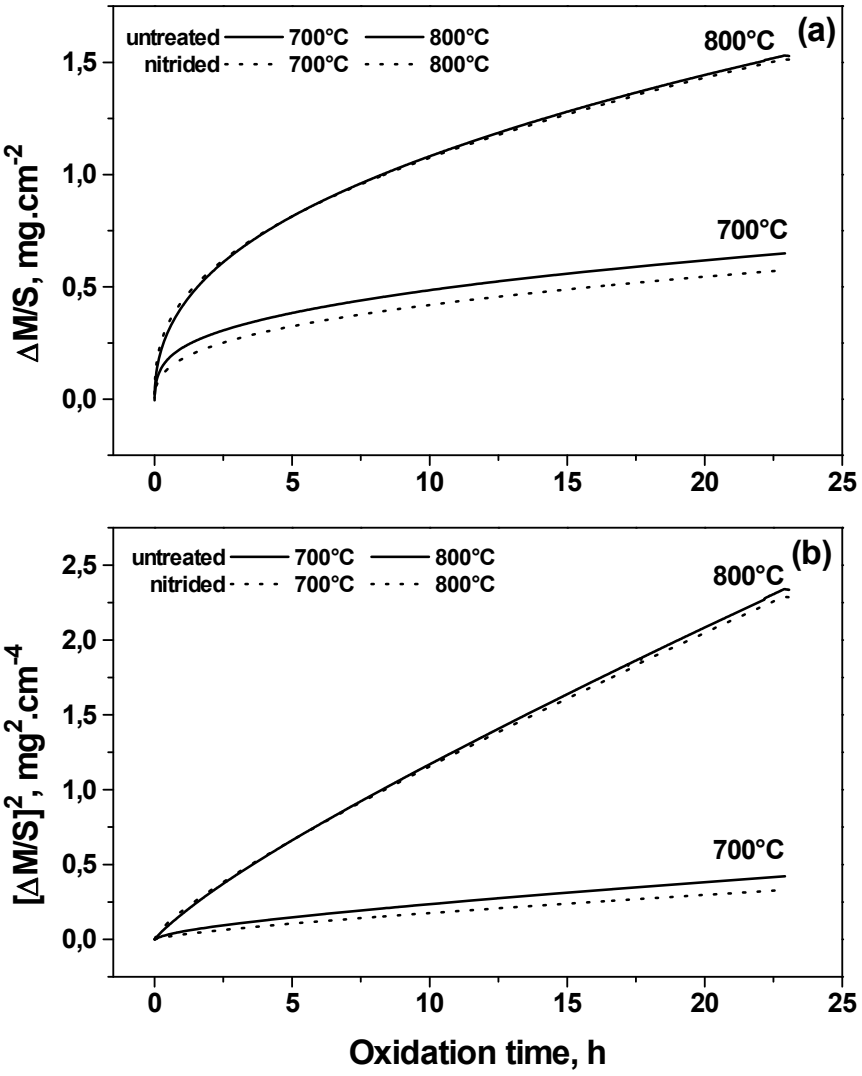

Figure 3.- Isothermal oxidation of nickel substrates at 700 and 800° C for 24 h in synthetic air. (a) Mass gain curves vs. time and (b) Square of the mass gain curves vs. time to calculate the parabolic rate constants. (N.B. Straight lines belong to untreated specimens whereas dot lines do for the nitrided samples).

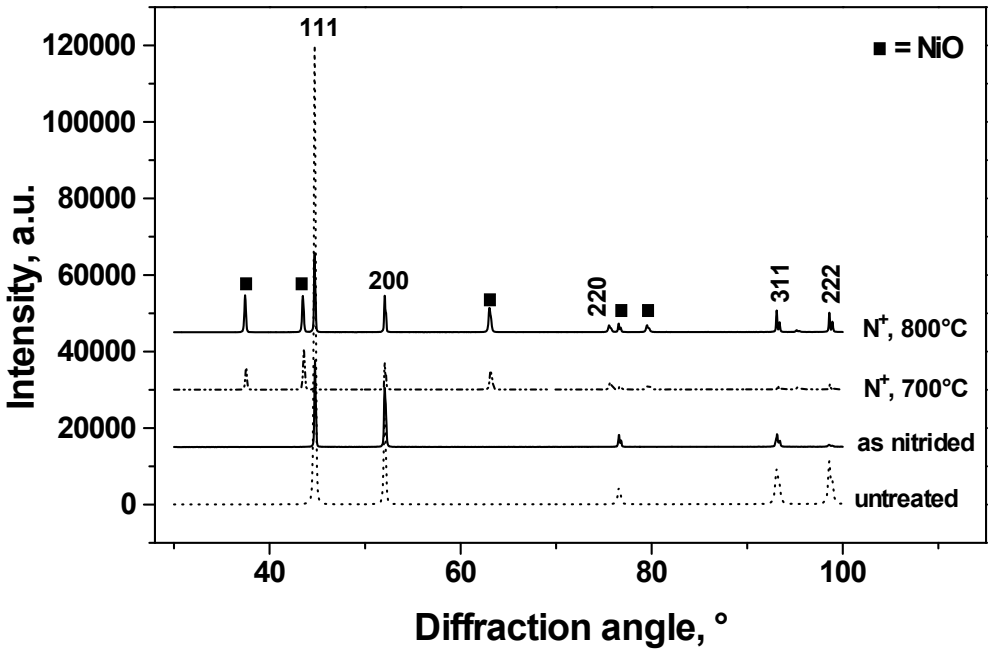

Figure 4.- XRD patterns of the untreated, nitrided and nitrided + oxidised Ni specimens. Oxidation was carried out at 700° and 800° C for 24 h under synthetic air. Squares represent the exclusive NiO formation.

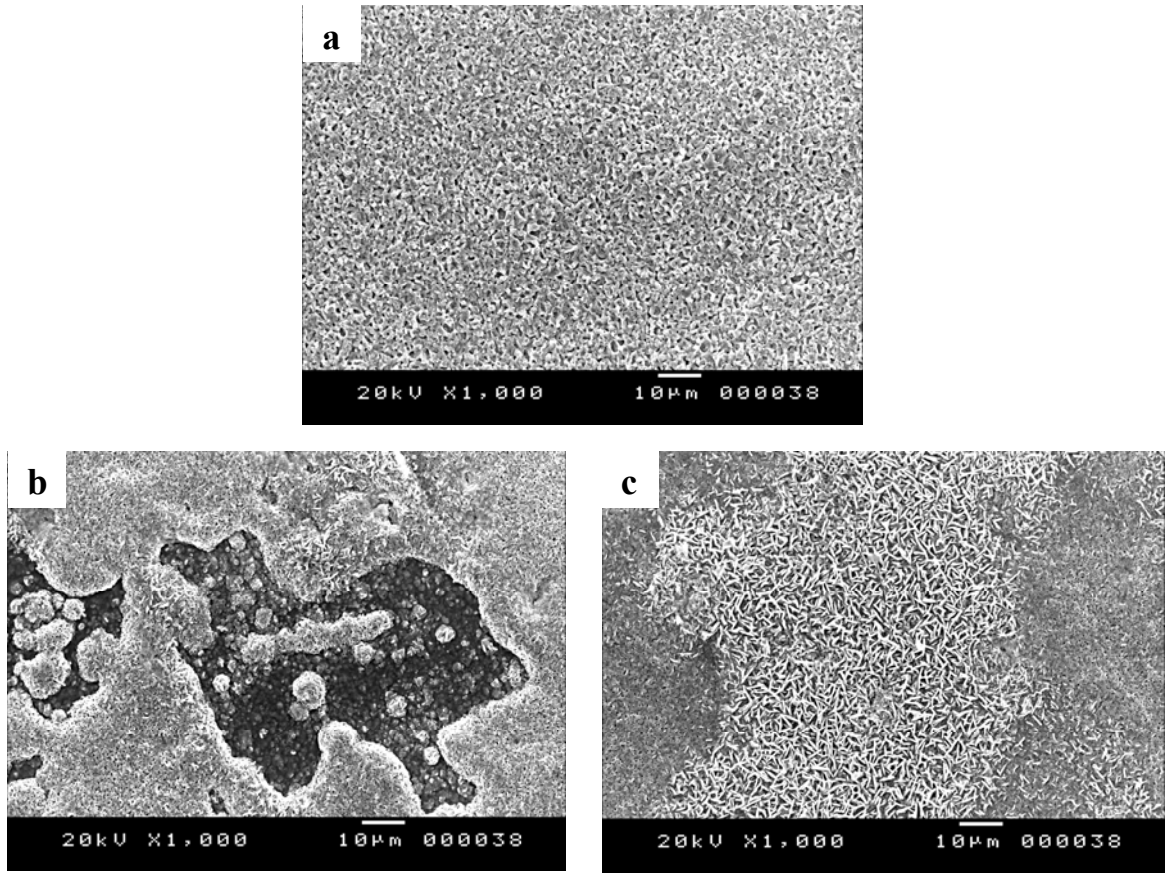

Figure 5.- SEM surface morphology developed on the Ni specimens (a) untreated and oxidised at 700°C and (b) and (c) nitrided and oxidised at 700° C.

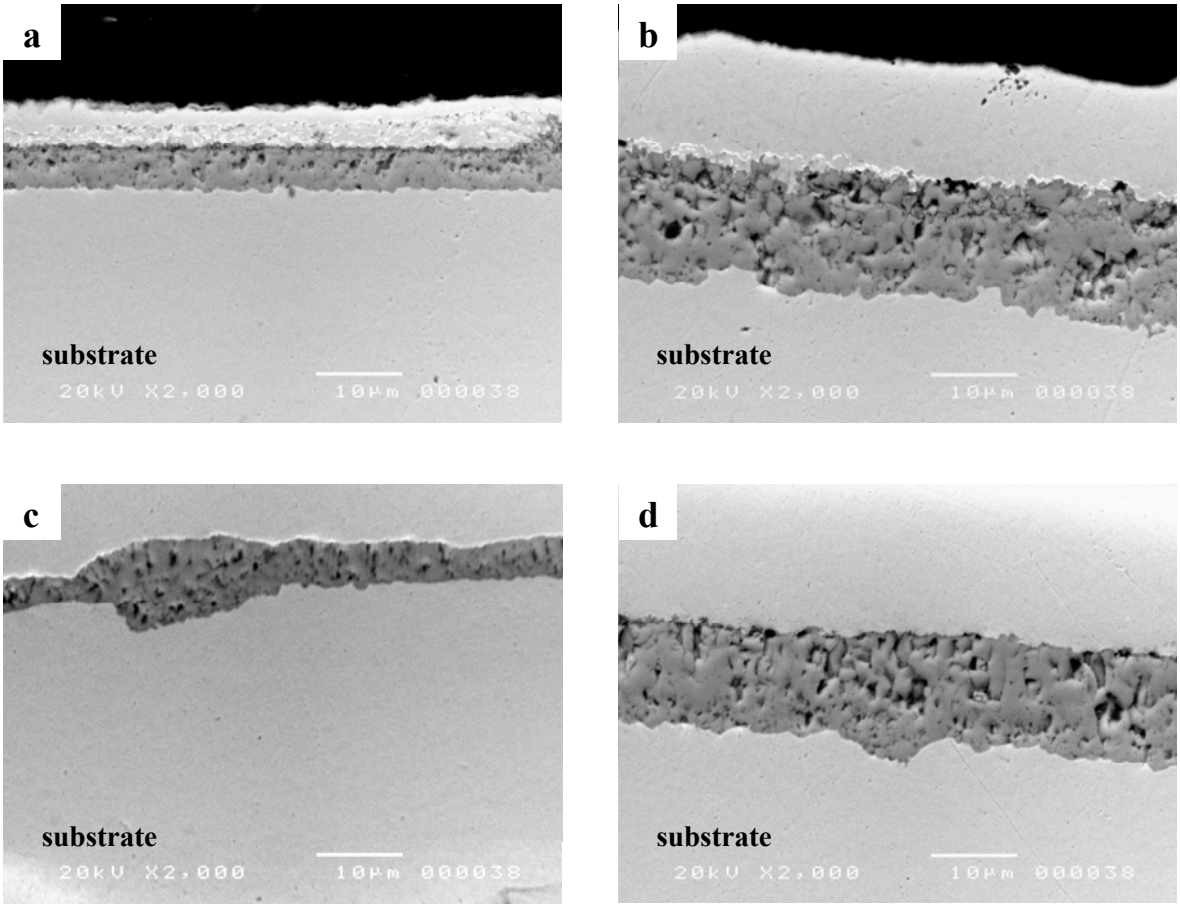

Figure 6.- SEM cross sections of the Ni specimens untreated and oxidised at (a) 700°C, (b) 800° C and nitrided and oxidised at (c) 700°C and (d) 800°C. (N.B. the layer over the oxide scales corresponds to electrolytically deposited nickel to protect the oxides).

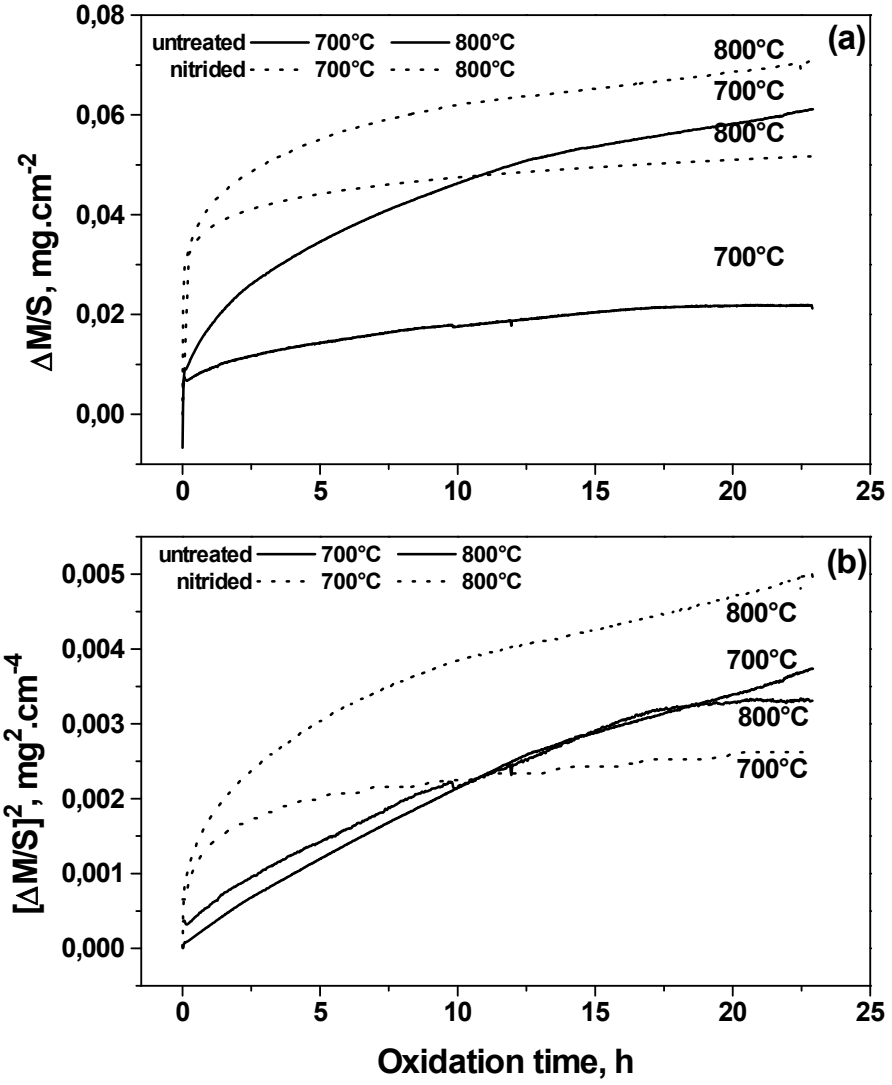

Figure 7.- Isothermal oxidation of Ni20Cr substrates at 700 and 800° C for 24 h in synthetic air. (a) Mass gain curves vs. time and (b) Square of the mass gain curves vs. time to calculate the parabolic rate constants. (N.B. Straight lines belong to untreated specimens whereas dot lines do for the nitrided samples).

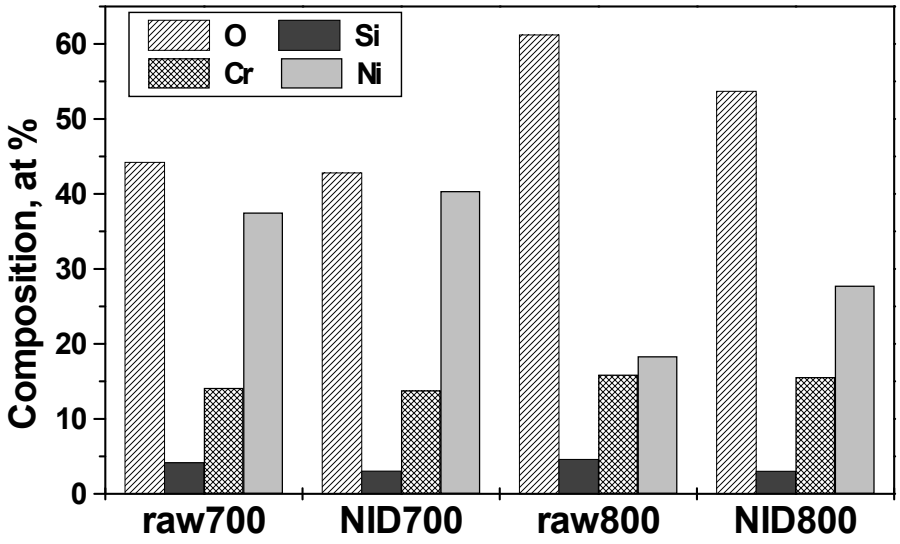

Figure 8. EDS surface composition analyses indicating the qualitative and semi-quantitative nature of the untreated (raw) and nitrided by implantation-diffusion (NID) Ni20Cr specimens subjected to isothermal oxidation at 700° and 800° C for 24 h.

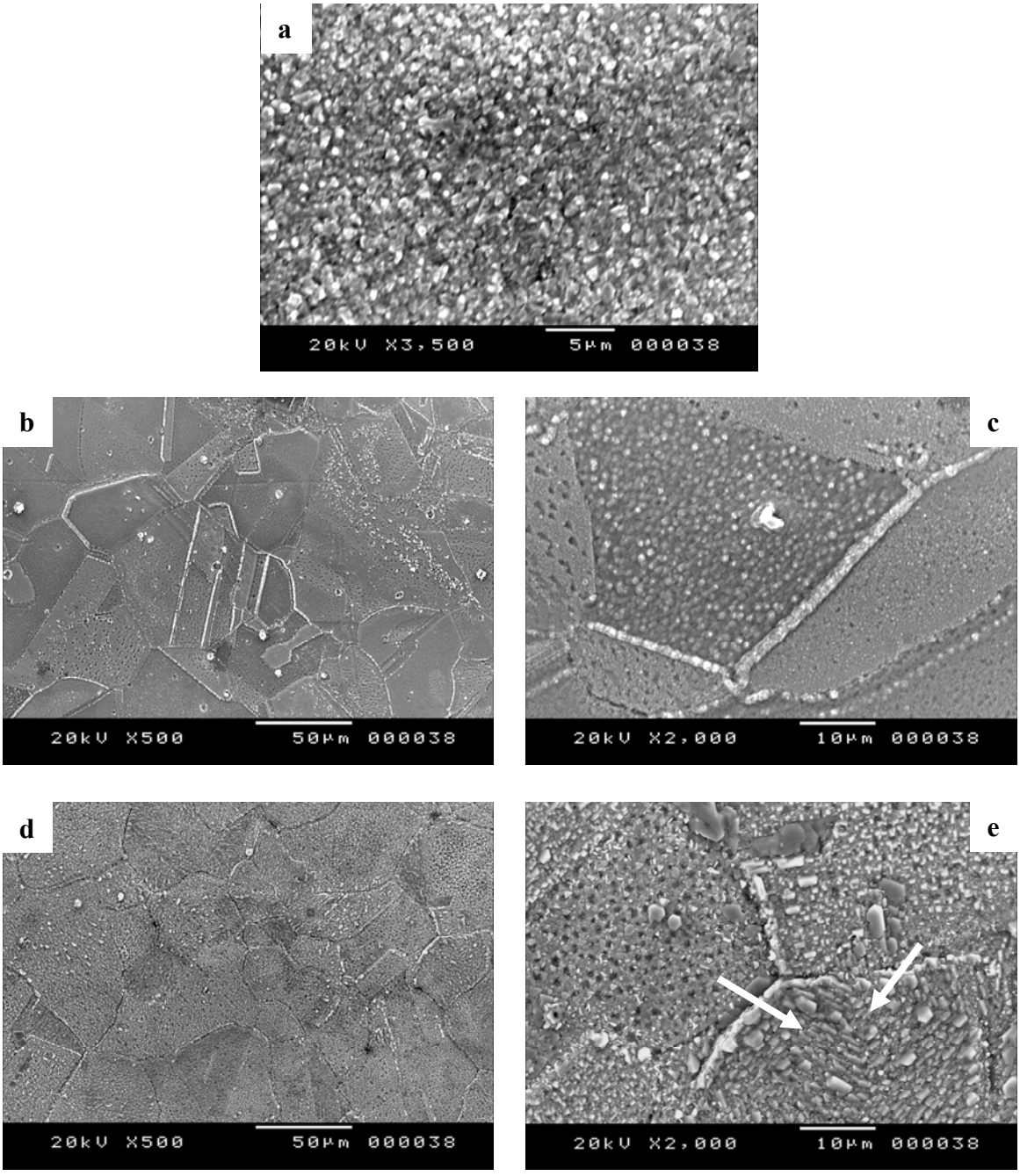

Figure 9. SEM surface morphologies of the Ni20Cr substrates after isothermal oxidation for 24 h of the (a) untreated and oxidised at 800°C and the nitrided and oxidised at (b) and (c) 700°C and (d) and (e) 800°C. Arrows indicate the growth direction of platelets.

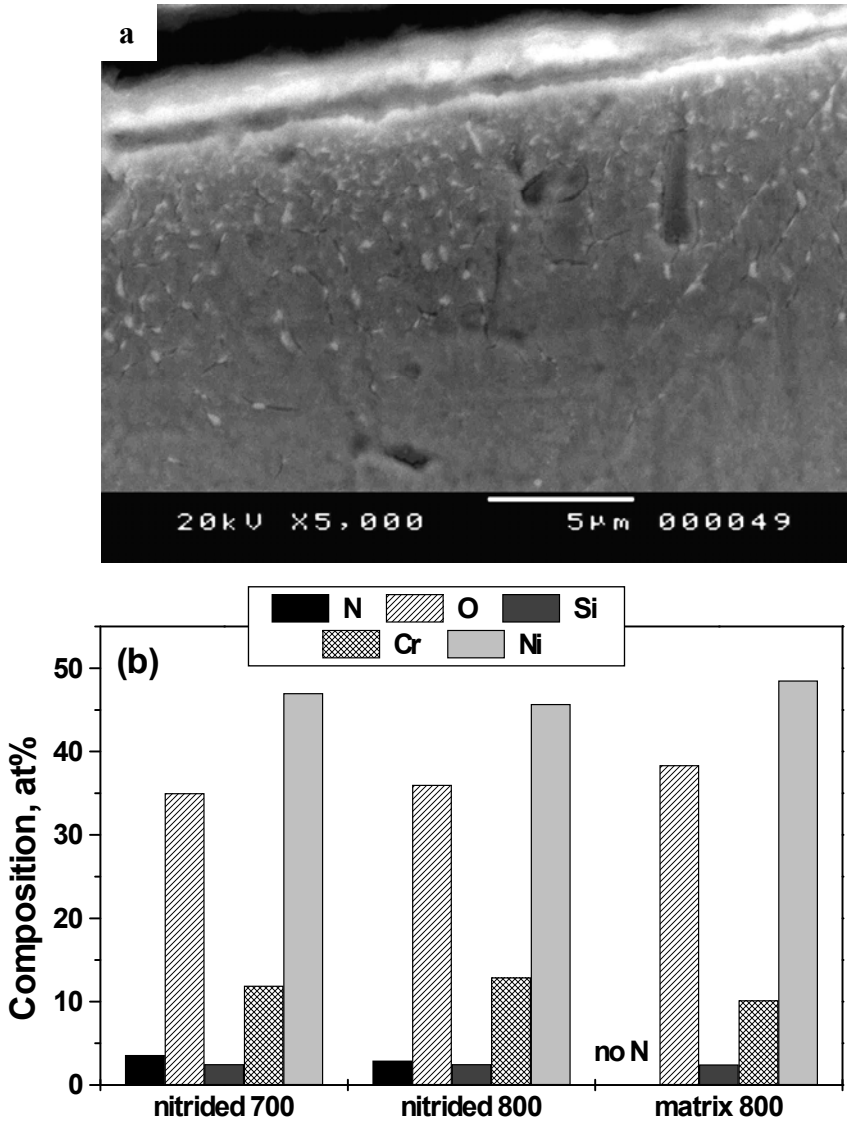

Figure 10. (a) SEM cross section of the nitrided Ni20Cr samples after isothermal oxidation at 800°C for 24 h showing precipitation beneath the oxide scale and (b) the EDS microanalyses obtained on the samples nitrided and oxidised at 700 and 800°C, showing the absence of nitrogen in the metal matrix.